JOURNAL OF CATALYSIS 116, 488–497 (1989)

Differences in the Promotional Effect of the Group IA Elements on Unsupported Copper Catalysts for Carbon Monoxide Hydrogenation

GORDON R. SHEFFER AND TERRY S. KING

Department of Chemical Engineering, Iowa State University, Ames, Iowa 50011

Received March 2, 1988; revised November 29, 1988

The differences in promotional effect of the Group IA elements on unsupported copper catalysts for carbon monoxide hydrogenation have been examined. Methanol was selectively produced on all catalysts at 523 K, 5 MPa, and with a feed gas of molar composition $H_2/CO = 2$. When normalized with respect to surface area, the methanol synthesis rate was found to increase by an order of magnitude from Li to Cs with the majority of the increase occurring from Na to K. On the basis of apparent activation energy measurements, X-ray photoelectron spectroscopy, and scanning electron microscopy results, activity differences were attributed to differences in the concentration of Cu^+ species at the surface and not to electronic effects. Alkali–cuprates, for example LiCuO, were determined not to be the active phase responsible for Cu^+ stabilization. Under conditions more favorable for higher alcohol synthesis, 573 K and $H_2/CO = 1$, little change in selectivity was observed for the Na-, K-, Rb-, and Cs-promoted catalysts. However, the lithium-promoted catalyst produced an equimolar mixture of normal alcohols and hydrocarbons. Both product distributions were found to give linear Flory plots with propagation constants of 0.3 for alcohols and 0.5 for hydrocarbons.

INTRODUCTION

The ability of potassium to promote unsupported copper for the synthesis of methanol from carbon monoxide and hydrogen has been reported previously (*1*). The role of potassium was to stabilize cuprous ions under reduction and reaction conditions. The mechanism of the potassium–copper interaction responsible for the formation of cuprous ions was not elucidated. However, phase formation was suggested as one possible mechanism for cuprous ion stabilization.

Klier and co-workers have reported that the Group IA elements also promote the synthesis of methanol over copper–zinc oxide catalysts (*2, 3*). The promotional effect increased monotonically from Li to Cs. At high temperatures and low H_2/CO ratios, the selectivity to higher alcohols was enhanced and increased from 6 wt% for Li to 15 wt% for Cs. At similar promotion levels and reaction conditions, except higher pressure, Smith and Anderson have reported selectivities to higher alcohols as great as 34 wt% for copper–zinc–aluminum oxide catalysts impregnated with potassium carbonate (*4*). Unlike molybdenum sulfide (*5, 6*) and copper–cobalt–chromium (*7, 8*), which are higher alcohol catalysts where the alcohol distribution is consistent with the Flory equation, alkali-promoted, copper–zinc oxide catalysts have an alcohol distribution that is better modeled by a chain growth scheme allowing for one to two carbon additions to the growing alcohol at the hydroxylated carbon atom or the carbon atom directly next to it (*4*). This scheme accounts for the high isobutanol fraction (up to 36%) found in the higher alcohol product. The ability of the Group IA elements to promote the higher alcohol synthesis for unsupported copper–alkali catalysts under conditions (high temperature, low H_2/CO ratio) favorable for higher alcohol formation has not been previously investigated.

In this study we have examined the difference in promotional effects of the Group

0021-9517/89 $3.00

IA elements on unsupported copper catalysts. Catalytic behavior was evaluated under both methanol synthesis conditions (523 K, $H_2/CO = 2$) and conditions more favorable for higher alcohol synthesis (573 K, $H_2/CO = 1$). The chemical nature of the catalyst was probed with X-ray photoelectron spectroscopy, powder X-ray diffraction, scanning electron microscopy, and apparent activation energy measurements. The role of alkali–cuprate compounds, for example, LiCuO, as active phases in the copper–alkali catalysts was also investigated.

EXPERIMENTAL

The method of catalyst preparation was similar to that outlined by Courty *et al.* (*8*) for alkali-promoted, copper–cobalt-based higher alcohol catalysts. Briefly, citric acid was added to an aqueous solution of alkali nitrate and cupric nitrate to yield one gram equivalent of acid per gram equivalent of copper and alkali ions. The resulting solution was vacuum evaporated at room temperature to form a thick slurry that was subsequently dried overnight at 353 K in a conventional convection oven. The solid obtained was calcined at 623 K in air for 4 h. It was observed that at approximately 473 K, catalyst precursors rapidly decomposed with the evolution of large amounts of heat and gas. Copper and alkali concentrations were verified by atomic absorption and flame emission spectroscopies of the calcined catalysts.

Catalysts were evaluated in a single-pass, fixed-bed microreactor system detailed elsewhere (*1*). All catalysts were reduced *in situ* before synthesis gas exposure by use of a 10% H_2 in argon gas mixture at 523 K ~ atmospheric pressure. A small temperature rise (10 to 15 K) was noted initially upon hydrogen exposure. Carbon monoxide conversions were less than 10 mol%, minimizing heat and mass transfer limitations as well as avoiding methanol equilibrium conditions. Surface areas of freshly reduced and used catalysts were determined from multipoint BET adsorption isotherms obtained with a Micromeretics 2100E Accusorb instrument using Kr at 77° K as the adsorbate.

Powder X-ray diffraction patterns were obtained with an automated Picker theta–theta diffractometer using Mo$K\alpha$ radiation. The step size was 0.04° per step with a counting time of 6s per step. Low-surface-area quartz (α-SiO_2), used as an internal standard, was mixed thoroughly with all samples at a concentration of 5 wt%. The *d*-spacing of the α-SiO_2 (101) reflection was referenced to 3.342 Å. To avoid sample exposure to air after reduction or synthesis gas exposure, a sample chamber utilizing a beryllium window was constructed. The design of the cell is shown in Fig. 1. Heating tape was used to heat the samples to reaction temperatures. To obtain reduced catalyst spectra, a flow of 10% H_2 in argon at atmospheric pressure was passed over the sample for 4 h. In studies where synthesis gas exposure was performed, the catalyst was first reduced as described above, and then a synthesis gas of molar composi-

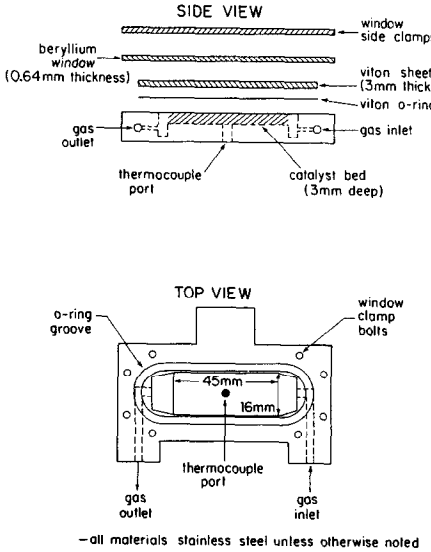

FIG. 1. Controlled atmosphere X-ray diffraction cell.

tion $H_2/CO = 2$ was passed over the catalyst at atmospheric pressure for up to 16 h.

X-ray photoelectron spectra were obtained with an AEI 200B spectrometer using Al$K\alpha$ radiation. Binding energies of the photoemitted electrons were assigned by referencing the carbon 1s peak of adventitious carbon to 285.0 eV. Samples were prepared by loading the catalyst into soda-lime glass tubing, by treating them with a 10% H_2 in argon gas mixture at atmospheric pressure and 523 K for 4 h, and then by evacuating and sealing the tubes. The tubes were then transported to and opened in a helium dry box attached directly to the spectrometer. XPS data were quantitated using the equation

$$X_i = (I_i/S_i)\Big/\Big(\sum_j I_i/S_i\Big),$$

where X_i, I_i, and S_i are the mole fraction, integrated intensity, and sensitivity factor of element i, respectively. The summation was performed over the j species observed in the XPS spectra. Sensitivity factors used were handbook values (*9*) except in the case of copper where the sensitivity factor was back-calculated using LiCuO as a reference compound.

RESULTS

Catalytic Behavior of Copper–Alkali Catalyst

The mole fraction of alkali relative to copper incorporated in the catalyst and the resulting catalyst surface areas are given in Table 1. Surface areas are reported for catalysts immediately following hydrogen pretreatment and after synthesis gas reaction. Catalyst surface areas are observed to decrease by a factor of 10 from Li to Cs.

The methanol synthesis activity of the copper–alkali catalysts is summarized in Table 2. Synthesis gas of molar composition $H_2/CO = 2$ was used at 523 K and 5 MPa. As reported previously (*1*), the unpromoted copper catalyst is inactive. For promoted catalysts, the selectivity to methanol was greater than 98 wt% in all cases except for Li where the selectivity was 90 mol%. Under these conditions, methane and ethanol were the primary by-products with traces of higher hydrocarbons for all catalysts. When expressed per weight of catalyst, the activity differences do not follow any trend. In addition, catalysts are observed to lose activity with time on stream until they reach steady-state values. However, when the data are compared on a surface area basis, the initial and steady-state activities are nearly the same indicating that sintering is fully responsible for the

TABLE 1

Composition and Surface Areas of Copper–Alkali Catalysts

Alkali	Mole fraction alkali[a]	Surface area (m^2/g)	
		Fresh	Used
None	0	—[b]	1.22
Li	0.40	1.73	1.04
Na	0.38	1.04	0.78
K	0.25	0.83	0.33
Rb	0.30	0.35	0.17
Cs	0.30	0.14	0.10

[a] Defined by mol alkali/(mol alkali + mol Cu).
[b] Not measured.

TABLE 2

Initial and Steady-State Methanol Synthesis Rates[a]

Alkali	Activity (kg/g cat/h) × 10^5		Activity ($kg/m^2/h$) × 10^5	
	Initial	Steady state	Initial	Steady state
None	0	<0.2	0	<0.2
Li	1.7	1.0	1.0	1.0
Na	1.6	1.4	2.0	2.1
K	9.6	5.1	12	15
Rb	4.9	3.1	14	18
Cs	2.6	1.4	18	14

[a] T = 523 K, P = 5 MPa, H_2/CO = 2, GHSV = 4000 h^{-1}.

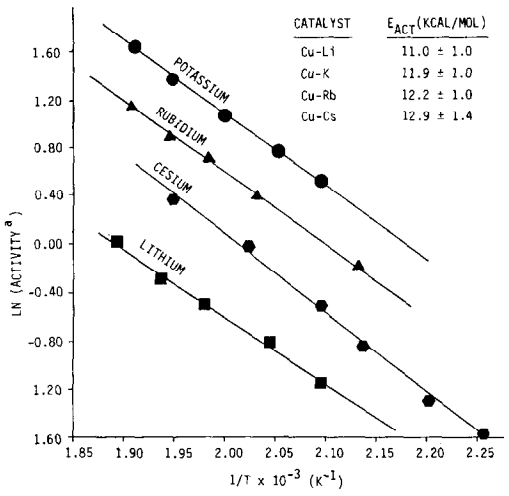

FIG. 2. Arrhenius plots for methanol synthesis on copper–alkali catalysts at 5 MPa and $H_2/CO = 2$.

activity decrease observed with time on stream. An order of magnitude increase in the surface area normalized activity was found descending the Group IA elements from Li to Cs with the majority of the increase occurring from Na to K.

Apparent activation energies for methanol synthesis were evaluated from the Arrhenius plots shown in Fig. 2. There is a small change in the apparent activation energy from Li, with an apparent activation energy of 11 kcal/mol, to Cs, with an apparent activation energy of 12.9 kcal/mol. These values are more typical of ones reported for supported Rh (*10–12*) or Pd (*13, 14*) catalysts than of alkali-promoted copper–zinc oxides, where a value of 18 kcal/mol has been reported for a cesium-promoted catalyst (*3*).

Increasing the reaction temperature to 573 K and lowering the H_2/CO molar ratio to unity had little effect on the selectivity except in the case of Li where a variety of hydrocarbons and alcohols was observed (see Table 3). Unlike alkali-promoted copper–zinc oxide catalysts where significant branching is observed (*4*), the higher alcohols formed were linear. Moreover, the alcohol and hydrocarbon distributions were consistent with Flory theory (see Fig. 3). The chain growth probability factors were substantially different with values of 0.30 for alcohols and 0.53 for hydrocarbons. When the mole fractions of both functionalities were combined, a chain growth probability factor of 0.37 was obtained.

TABLE 3

Activity and Selectivity of Copper–Alkali Catalysts under Higher Alcohol Synthesis Conditions[a]

Alkali	Activity × 10^3 (mol CO/m²/h)	Selectivity (mol %)				
		Hydrocarbons		Alcohols		
		C_1	C_2^+	C_1	C_2	C_3^+
Li	0.6	31.1	18.7	40.8	6.9	2.5
Na	0.3	10.6	2.4	87.0	—	—
K	2.3	1.4	—	98.0	0.6	—
Rb	3.5	1.4	0.3	98.2	0.1	—
Cs	9.3	2.2	0.7	96.8	0.4	—

[a] T = 573 K, P = 5 MPa, H_2/CO = 1, GHSV = 4000 h^{-1}.

Characterization of Copper–Alkali Catalysts

X-ray powder diffraction patterns for the copper–alkali series revealed copper metal to be the only bulk copper phase present. The lattice parameters for the copper metal

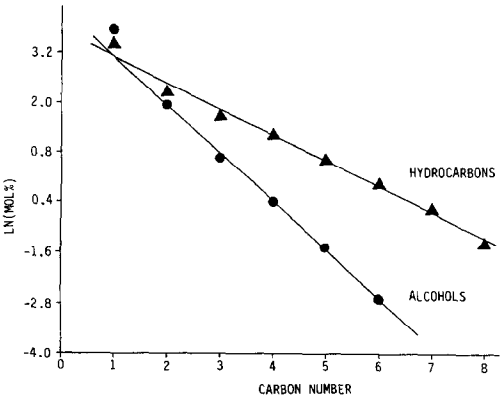

FIG. 3. Flory plot of alcohols and hydrocarbons produced on Cu–Li catalyst at 573 K, 5 MPa, and H_2/CO = 1.

in the catalyst agreed well with those reported for pure copper metal in the literature (*15*). A very weak pattern corresponding to the various alkali carbonates was also observed. As we have noted previously for a copper–potassium catalyst (*1*), most of the alkali in the catalyst is invisible to this technique, indicating that the alkali is in either a microcrystalline (<20 Å) or an amorphous phase. Scanning electron microscopy coupled with energy-dispersive spectroscopy of reduced copper–alkali catalysts revealed no areas of unusually high alkali concentrations such as have been observed with certain preparations of copper–potassium catalysts (*1*). For each catalyst, the copper-to-alkali ratio was constant from particle to particle, indicating that the alkali was homogeneously distributed.

In order to evalaute the chemical state of copper at the surface, X-ray photoelectron spectroscopy of reduced catalyst samples was performed. The use of reduced catalysts instead of synthesis gas-treated samples is justified by the excellent initial activity of the catalysts. Examination of the Cu $2p_{3/2}$ region revealed only one peak at a binding energy of 931.5 eV for the Na, K, Rb, and Cs catalysts and at 930.3 eV for the Li-promoted catalyst. The Cu $2p_{3/2}$ peak had no satellite structure and was assigned to Cu^+ or Cu^0 species. Differentiation of Cu^+ or Cu^0 species was performed by examination of the positions of the $L_3M_{4,5}M_{4,5}$ Auger transition relative to the Cu $2p_{3/2}$ position. Figure 4 is a plot of the $L_3M_{4,5}M_{4,5}$ region for the copper–alkali series. The abscissa of Fig. 4 is referred to as the modified Auger parameter (*16*) and is defined by

$$\alpha + h\nu = KE_{LMM} - BE_{2p_{3/2}}.$$

The Auger parameter, α, is the difference of the kinetic energy of the LMM Auger transitions (KE_{LMM}) and the kinetic energy of the $2p_{3/2}$ photoemitted electron ($KE_{2p_{3/2}}$). The addition of $h\nu$, the excitation energy, to α allows for the modified Auger parameter to be independent of the excitation energy since $h\nu - KE_{2p_{3/2}}$ is simply the binding energy of the $2p_{3/2}$ photoemitted electron. The advantage of using Auger parameters is that static charging effects subtract out. The peaks at 1848.8 and 1850.6 eV correspond to Cu^+ and Cu^0 species, respectively. The extra peak at 1853 eV for the sodium-promoted catalyst is the $NaKL_1L_1$ Auger transition.

The presence of carbonate species was also detected in the C 1*s* spectra. The binding energies of the C 1*s* line for the catalysts are listed in Table 4. The 289.7 eV value for the copper–sodium catalyst agrees well with that reported for sodium carbonate

TABLE 4

C 1*s* Binding Energies of Carbonate Species in Copper–Alkali Catalysts

Alkali	C-1*s* binding energy (eV)
Li	291.4
Na	289.7
K	289.2
Rb	289.0
Cs	288.9

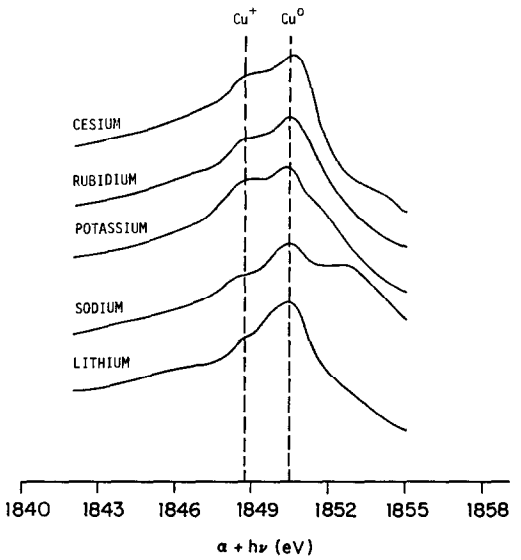

FIG. 4. $L_3M_{4,5}M_{4,5}$ X-ray-induced Agar transitions for reduced copper–alkali catalysts.

TABLE 5

Surface Concentration of Cu^+ and Stoichiometry of Alkali, Oxygen, and Carbon (as Carbonate) as Determined by XPS

Catalyst	Mole fraction Cu^+	Alkali, oxygen, and carbon stoichiometry
Cu–Li	0.006	$Li_{2.1}C_{0.91}O_3$
Cu–Na	0.018	$Na_{2.2}C_{0.87}O_3$
Cu–K	0.048	$K_{1.9}C_{0.87}O_3$
Cu–Rb	0.050	$Rb_{1.8}C_{1.07}O_3$
Cu–Cs	0.064	$Cs_{1.8}C_{1.01}O_3$

(*17*). The observed decrease in the C 1*s* binding energy of the carbonate species when descending from Li to Cs corresponds with the decrease in electronegativity.

The surface concentrations of copper, alkali, oxygen, and carbon (as carbonate) were determined using methods described earlier. Although Cu^+ and Cu^0 have the same Cu $2p_{3/2}$ binding energy, it was possible to evaluate their respective surface concentrations by calculating the proportion of copper as Cu^+ and Cu^0 from integration of the $L_3M_{4,5}M_{4,5}$ Auger transitions. This method of determining the Cu^+ and Cu^0 concentrations was warranted by the observation that Cu^+ (as LiCuO) and Cu^0 metal had identical sensitivity factors and Cu–$L_3M_{4,5}M_{4,5}$ to Cu $2p_{3/2}$ integrated intensity ratios. When the XPS data were quantitated, two items became evident (see Table 5). First, the concentration of Cu^+ at the surface of the copper–alkali catalysts was found to increase in the order Li < Na < K < Rb < Cs. Second, the concentration of alkali, oxygen, and carbon (as carbonate) was very close to stoichiometric for alkali carbonate.

Preparation and Characterization of LiCuO

One possible phase that accounts for the formation of cuprous ions in copper–alkali catalysts is that of alkali–copper oxides that have been synthesized and characterized by Hestermann and Hoppe (*18*), Hoppe *et al.* (*19*), and Klassen and Hoope (*20*). In order to understand what role, if any, these compounds may play in the synthesis of methanol, LiCuO was prepared. LiCuO was chosen over the other alkali–cuprate oxides because of the surprising product distribution observed for the Cu–Li catalysts at higher temperatures and a low H_2/CO ratio.

We prepared LiCuO by heating a mixture of Li_2O (Pfaultz and Bauer, 95%) and Cu_2O (Cerac, 99.9%) in quartz tubing under vacuum at 1113 K for 12 h (*21*). Ten mole percent excess Li_2O was added to the initial mixture. After heating, unreacted Li_2O was removed by washing the product with anhydrous methanol. The powder X-ray diffraction pattern revealed only LiCuO to be present. LiCuO is yellow and hydrolyzes in air.

The catalytic behavior of LiCuO at 523 K is summarized in Table 6. the selectivity to methanol was 99 wt%. The steady-state activity of LiCuO was comparable to that for the Cu–Li catalyst. However, the initial activity was only 15% of the steady-state activity, suggesting that LiCuO was modified by synthesis gas exposure. At 573 K and a H_2/CO ratio of unity, the selectivity to methanol was still approximately 99 wt%. To help elucidate the changes in the chemical nature of LiCuO that occurred upon

TABLE 6

Comparison of Catalytic Behavior of Cu–Li Catalysts with CuLiO[a]

Catalyst	Surface area (m^2/g)		Activity (kg $CH_3OH/m^2/h$)	
	Fresh	Used	Initial	Steady state
Cu–Li	1.73	1.04	1.0×10^{-5}	1.0×10^{-5}
CuLiO	2.32	1.68	0.3×10^{-5}	2.0×10^{-5}

[a] T = 523 K, P = 5 MPa, H_2/CO = 2, GHSV = 4000 h^{-1}.

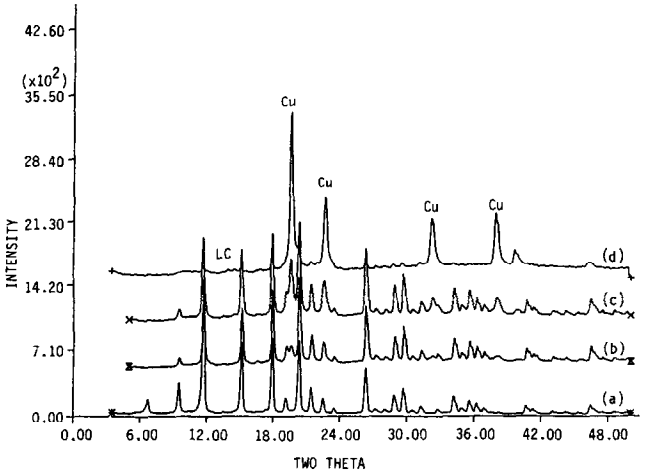

FIG. 5. X-ray diffraction patterns of LiCuO after hydrogen and synthesis gas exposure: (a) no treatment, (b) after 6 h of hydrogen exposure, (c) after 2 h of synthesis gas exposure, (d) after 16 h of synthesis gas exposure.

synthesis gas exposure, we employed X-ray diffraction. The diffraction patterns shown in Fig. 5 were collected in the sample chamber described earlier. LiCuO was treated with synthesis gas for 2-h intervals at atmospheric pressure and 523 K. Between intervals the cell was purged with helium and transferred to the diffractometer for analysis. At no time were the contents of the cell exposed to the atmosphere. Before synthesis gas exposure, LiCuO was treated with pure hydrogen for 6 h at 0.1 MPa and 523 K. The diffraction pattern obtained after hydrogen treatment was identical to that for LiCuO except for the small peaks marked "Cu," which were due to copper metal. Overall, LiCuO was relatively stable under a hydrogen atmosphere at 523 K. After 2 h of synthesis gas exposure, the amount of copper metal increased dramatically. After 16 h of this exposure, only a trace of LiCuO remained. Additionally, a small amount of lithium carbonate, denoted "LC," was found. It is surprising that despite the presence of an equimolar amount of lithium to copper, the lithium disappeared from the diffraction pattern in a manner similar to that of the alkali-promoted copper catalysts. The $L_3M_{4,5}M_{4,5}$ X-ray-induced Auger spectrum of synthesis-gas-exposed LiCuO was similar to that shown in Fig. 4 for the Cu–Li catalyst. The binding energy of the Cu $2p_{3/2}$ emission was 931.7 eV, similar to that found for the Na-, K-, Rb-, and Cs-promoted catalysts.

DISCUSSION

The methanol synthesis rate, normalized with respect to surface area, on unsupported copper–alkali catalysts was found to increase by an order of magnitude progressively from Li to Cs. Interestingly, most of this increase occurs from Na to K with the activity of Li- and Na-promoted catalysts being comparable and that of K-, Rb-, and Cs-promoted catalysts being comparable. The steady-state methanol synthesis rate for the K-, Rb-, and Cs-promoted copper catalysts was approximately 15×10^{-5} kg/m²/h, which is a factor of 5 greater than the 3×10^{-5} kg/m²/h value reported for a Cs-promoted, copper–zinc oxide catalyst at 523 K, 7.5 MPa, with a synthesis gas of molar composition $H_2/CO = 2.3$ (*3*). The apparent activation energies for the catalyst series are only different by 1.9 kcal/mol,

which is within the limits of experimental error. Although the values are within experimental error, there is a definite decreasing trend in activation energies from Li to Cs. Vedage *et al.* (*2*) have proposed that the role of alkali ions in alkali-promoted, copper–zinc oxide catalysts is to allow for methanol production through hydrogenation of alkali formate intermediates produced by the reaction of alkali hydroxide with carbon monoxide. The increase in methanol production from Li to Cs was hypothesized to result from the corresponding increase in basicity. One would therefore expect that if alkali formates were important intermediates in methanol synthesis for the catalysts of interest here, then the activation energy would decrease from Li to Cs. However, if the alkali compounds present in the catalyst were donating electron density to Cu^+ species, presumably the active site in methanol synthesis (*22, 23*) to make the catalyst more metallic-like, then the activation energy would increase. The increasing activation energy found in the work presented here, coupled with the presence of Cu^+ species detected via XPS, is consistent with this latter explanation.

As shown in Fig. 6, the initial rate of methanol synthesis, normalized with respect to surface area, correlates with the concentration of Cu^+ at the surface as determined by XPS. Since the SEM/EDS results indicated that the alkali is homogeneously distributed throughout the catalyst, the increase in Cu^+ concentration is interpreted to be an indication that K, Rb, and Cs are more capable of forming the Cu^+ species than Li and Na. A similar conclusion has been reached using ^{65}Cu NMR (*24*). Considering that the increase in activation energy from Li to Cs would tend to decrease the rate of methanol synthesis, the increase in activity from Li to Cs must be attributed to differences in the concentration of active sites and not to electronic effects.

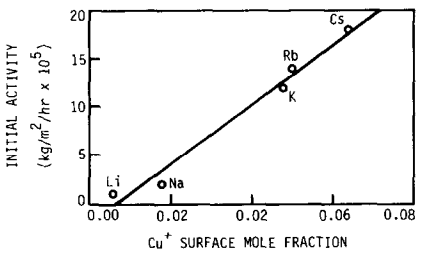

FIG. 6. Rate of methanol synthesis as a function of Cu^+ concentration as determined by XPS.

The mechanism by which Cu^+ species are stabilized in the catalyst is indicated by the work reported here. The poor initial activity and subsequent decomposition of LiCuO upon synthesis gas exposure eliminates alkali–cuprates as possible active phases. XPS results indicate that the alkali component of the catalysts is present only in the carbonate phase. One could speculate that the stabilization of cuprous ions occurs by formation of a mixed metal carbonate, for example, $KCuCO_3$. Although the synthesis of alkali–copper carbonates has not been reported in the literature, the synthesis of alkali–silver carbonates has been noted (*25*). Subsequent work with NMR of ^{133}Cs in the cesium-promoted catalyst supports this view (*24*).

The behavior of the Cu–Li catalysts under higher alcohol synthesis conditions (573 K, $H_2/CO = 1$) was quite unexpected. Whereas alkali-promoted, copper–zinc oxide catalysts retain high alcohol selectivity and produce a large fraction of branched alcohols, the Cu–Li catalyst produced a Flory distribution of normal alcohols and normal hydrocarbons more typical of alkali-promoted, copper–cobalt–chromium oxide catalysts (*8*). Chen *et al.* (*26*) have reported that the activity of copper-supported Cr_2O_3 or ZrO_2 for carbon monoxide hydrogenation is a factor of 20–40× greater than that for bulk copper. The withdrawal of electron density from copper by the supports, which are *p*-type semiconductors, was proposed to alter the chemical nature of copper to a state somewhere between Cu^0 and Cu^+. In our study, an indication of

electron donation to copper from lithium is observed by the 1.2-eV decrease in the Cu $2p_{3/2}$ binding energy. Since alkali carbonates are basic compounds, they would be expected to donate electron density to copper. The increased electron density on copper could increase the chemisorption strength of carbon monoxide, resulting in increased carbon monoxide dissociation and Fischer–Tropsch activity. The synthesis of higher alcohols could occur either directly on the electronically modified copper metal sites or by interaction of alkyl chains on those sites with Cu^+ sites stabilized by phase formation.

Two questions become evident from the results reported here. First, why do the other alkali–copper catalysts retain high methanol selectivity? One simple explanation is that the increased size of the other alkalis compared to lithium could lead to increased site blocking. Second, why was the LiCuO preparation not observed to catalyze the synthesis of higher alcohols and hydrocarbons? Here, the concentration or dispersion of lithium at the surface may play a role, especially if the interaction between copper and lithium is localized.

In any case, the copper–lithium catalyst system will require further investigation for us to understand fully the interaction of copper with alkali promoters. Initially it would appear that two methods of promotion occur here. The first is phase formation to stabilize Cu^+ species for methanol synthesis, and the second is perhaps an electronic interaction resulting in electron donation to copper metal that causes Fischer–Tropsch-type behavior.

SUMMARY

The rate of methanol synthesis on unsupported copper–alkali catalysts, normalized with respect to surface area, increased by an order of magnitude from Li to Cs, with most of the increase occurring from Na to K. A 1.9 kcal/mol increase in the apparent activation energy was observed across the series. X-ray photoelectron spectroscopy results indicated the presence of Cu^+ species at the catalyst surface. Activity differences were attributed to differences in the concentration of Cu^+ sites at the surface and not to electronic effects.

The alkali–cuprate LiCuO was prepared and investigated with respect to its role as an active phase. The compound exhibited poor initial activity, although steady-state activity was comparable to the Cu–Li catalyst prepared by citrate complexation. X-ray diffraction studies indicated that LiCuO decomposed under synthesis gas to a mixture of copper metal and lithium carbonate. LiCuO as an active phase is discounted, and copper–alkali carbonates are proposed.

Under higher alcohol synthesis conditions (573 K and $H_2/CO = 1$), the selectivity of the Na-, K-, Rb-, and Cs-promoted copper catalysts did not change, but an equimolar mixture of hydrocarbons and alcohols was produced by the Cu–Li catalyst. Both the hydrocarbon and the alcohol distributions gave linear Flory plots with propagation constants of 0.3 for alcohols and 0.5 for hydrocarbons. X-ray photoelectron spectroscopy results indicated that the electron density of copper was greater with lithium as the promoter than the other Group IA elements. Further investigation will be required for us to understand fully the interactions between lithium and copper that are responsible for the synthesis of higher alcohols.

ACKNOWLEDGMENTS

The authors gratefully acknowledge the receipt of start-up funds from the Faculty Initiation Fund of the Shell Companies Foundation. One of the authors (G.R.S.) thanks the Amoco Foundation for fellowship support. In addition, we thank Dr. Robert Jacobson (Ames Laboratory) for use of the X-ray diffractometer and James Anderegg (Ames Laboratory) for assistance in the collection of X-ray photoelectron spectra.

REFERENCES

1. Sheffer, G. R., and King, T. S., *J. Catal.*, in press.
2. Vedage, G. A., Himelfarb, P. B., Simmons, G. W., and Klier, K., *in* "Solid State Chemistry in Catalysis," ACS Symposium Series 279, pp. 295–

312. American Chemical Society, Washington, DC, 1985.
3. Nunan, J. G., Klier, K., Young, C.-W., Himelfarb, P. B., and Herman, R. G., *J. Chem. Soc. Chem. Commun.*, 193 (1986).
4. Smith, K. J., and Anderson, R. B., *Canad. J. Chem. Eng.* **61,** 40 (1983).
5. Quarderer, G. J., and Cochran, G. A., European Patent Appl. 0,119,609 (1984).
6. Dianis, W. P., *Appl. Catal.* **30,** 99 (1987).
7. Sugier, A., and Freund, E., U.S. Patent 4,122,110 (1978).
8. Courty, P., Durand, D., Freund, E., and Sugier, A., *J. Mol. Catal.* **17,** 241 (1982).
9. "Handbook of X-Ray Photoelectron Spectroscopy" (G. C. Muilenberg, Ed.). Physical Electronics, Eden Prairie, MN, 1976.
10. Ichikawa, M., *Bull. Chem. Soc. Japan* **51,** 2268 (1978).
11. Chuang, S. C., Goodwin, J. G., and Wender, I., *J. Catal.* **95,** 435 (1985).
12. Gilhooley, K., Jackson, S. D., and Rigby, S., *Appl. Catal.* **21,** 349 (1986).
13. Ichikawa, M., *Shokubai* **21,** 253 (1979).
14. Ryndin, Y. A., Hicks, R. F., Bell, A. T., and Yermakov, Y. I., *J. Catal.* **70,** 287 (1981).
15. Joint Committee on Powder Diffraction Standards, file No. 4-0838.
16. Gaarenstrom, S. W., and Winograd, N., *J. Chem. Phys.* **67,** 3500 (1977).
17. Gelius, U., Heden, P. F., Hedman, J., Lindberg, B. J., Manne, R., Nordberg, R., Nordling, C., and Siegbahn, K., *Phys. Scr.* **2,** 70 (1970).
18. Hestermann, K., and Hoppe, R., *Z. Anorg. Allg. Chem.* **360,** 113 (1968).
19. Hoope, R., Hestermann, K., and Schenk, F., *Z. Anorg. Allg. Chem.* **367,** 276 (1969).
20. Klassen, H., and Hoppe, R., *Z. Anorg. Allg. Chem.* **485,** 101 (1982).
21. Migeon, H. N., Zanne, M., Gleitzer, C., and Courtois, A., *J. Solid State Chem.* **16,** 325 (1976).
22. Herman, R. G., Klier, K., Simmons, G. W., Finn, B. P., Bulko, J. B., and Kobylinski, T. P., *J. Catal.* **56,** 407 (1979).
23. Apai, G. R., Monnier, J. R., and Hanrahan, M. J., *J. Chem. Soc. Chem. Commun.*, 212 (1984).
24. Chu, P. J., Gerstein, B. C., Sheffer, G. R., and King, T. S., *J. Catal.* **115,** 194 (1989).
25. Papin, G., Christmann, M., and Sadeghi, N., *C.R. Acad. Sci. Ser. C* **284,** 791 (1977).
26. Chen, H.-W., White, J. M., and Ekerdt, J. G., *J. Catal.* **99,** 293 (1986).